doi:10.1093/brain/awr047 Brain 2011: 134; 1400–1415 | 1400

BRAIN
A JOURNAL OF NEUROLOGY

Overexpression of the autophagic beclin-1 protein clears mutant ataxin-3 and alleviates Machado–Joseph disease

Isabel Nascimento-Ferreira,[1,2,3] Tiago Santos-Ferreira,[4] Lígia Sousa-Ferreira,[1,2] Gwennaëlle Auregan,[3,5] Isabel Onofre,[1,2] Sandro Alves,[1,2,3] Noëlle Dufour,[3,5] Veronica F. Colomer Gould,[6] Arnulf Koeppen,[7] Nicole Déglon[3,5] and Luís Pereira de Almeida[1,2]

1 Center for Neurosciences and Cell Biology, University of Coimbra, 3004-517 Coimbra, Portugal
2 Faculty of Pharmacy, University of Coimbra, 3000-548 Coimbra, Portugal
3 CEA, Institute of Molecular Imaging (I2BM) and Molecular Imaging Research Center, 92265 Fontenay-aux-Roses, France
4 Department of Life Sciences, Faculty of Sciences, University of Coimbra, 3001-401 Coimbra, Portugal
5 CNRS/CEA URA2210, Fontenay-aux-Roses, France
6 Centro de Investigación y de Estudios Avanzados del Instituto Politécnico Nacional, 07360 México DF, México
7 Department of Neurology, VA Medical Center and Albany Medical College, 12208 Albany, NY, USA

Correspondence to: Luis Pereira de Almeida,
Center for Neurosciences and Cell Biology,
University of Coimbra,
Largo Marquês de Pombal,
3004-517 Coimbra,
Portugal.
E-mail: luispa@ci.uc.pt; luispa@cnc.uc.pt

Machado–Joseph disease, also known as spinocerebellar ataxia type 3, is the most common of the dominantly inherited ataxias worldwide and is characterized by mutant ataxin-3 misfolding, intracellular accumulation of aggregates and neuronal degeneration. Here we investigated the implication of autophagy, the major pathway for organelle and protein turnover, in the accumulation of mutant ataxin-3 aggregates and neurodegeneration found in Machado–Joseph disease and we assessed whether specific stimulation of this pathway could mitigate the disease. Using tissue from patients with Machado–Joseph disease, transgenic mice and a lentiviral-based rat model, we found an abnormal expression of endogenous autophagic markers, accumulation of autophagosomes and decreased levels of beclin-1, a crucial protein in the early nucleation step of autophagy. Lentiviral vector-mediated overexpression of beclin-1 led to stimulation of autophagic flux, mutant ataxin-3 clearance and overall neuroprotective effects in neuronal cultures and in a lentiviral-based rat model of Machado–Joseph disease. These data demonstrate that autophagy is a key degradation pathway, with beclin-1 playing a significant role in alleviating Machado–Joseph disease pathogenesis.

Keywords: Machado–Joseph disease; ataxin-3; autophagy; beclin-1; neuroprotection

Abbreviations: Atg = autophagic related protein; DARPP-32 = dopamine-and-cyclic AMP-regulated phosphoprotein of 32 kDa; p62 = sequestosome 1/p62 protein

Received August 16, 2010. Revised January 30, 2011. Accepted February 1, 2011. Advance Access publication April 7, 2011

Introduction

Machado–Joseph disease, also known as spinocerebellar ataxia type 3, is an autosomal dominant neurodegenerative disorder caused by a CAG trinucleotide repeat expansion within the coding region of the *MJD1* gene (Kawaguchi *et al*., 1994; Zoghbi, 2000). This gene encodes ataxin-3, a polyubiquitin-binding protein whose physiological function has been linked to ubiquitin-mediated proteolysis (Doss-Pepe *et al*., 2003; Chai *et al*., 2004). The polyglutamine tract confers a toxic gain-of-function to the mutant protein leading to neuronal dysfunction and cell death (Zoghbi, 2000; Duenas *et al*., 2006). The mutant protein accumulates and forms neuronal intranuclear inclusions. If these inclusions are hallmarks of the disease (Schmidt *et al*., 1998), their exact role in the polyglutamine pathology is still unclear.

There is strong evidence that proteins with a mutant polyglutamine tract are inefficiently degraded by the ubiquitin-proteosome system but may be degraded by macroautophagy (hereafter called autophagy), a mechanism with a crucial role in degradation of insoluble aggregate-prone proteins and essential for neuronal survival (Cuervo, 2004; Williams *et al*., 2006). Mice lacking either one of the autophagic genes 5 or 7 (*ATG5*/*ATG7*) develop neurodegeneration and cytoplasmic ubiquitinated aggregates, similarly to what happens in neurodegenerative disorders (Hara *et al*., 2006; Komatsu *et al*., 2006). Furthermore, the activity of this pathway decreases with ageing (Cuervo, 2004; Vellai, 2009) and is affected in several neurodegenerative diseases (Shibata *et al*., 2006; Pickford *et al*., 2008; Crews *et al*., 2010). Although autophagy was initially considered as a non-specific 'in-bulk' clearance mechanism, recent evidence supports selectivity of this process, with specific molecules recognizing polyubiquitination as a signal for cargo sequestration and autophagic clearance. The sequestosome 1/p62 protein (p62) was the first cargo-recognizing molecule identified, with a domain that binds both cargo and autophagic machinery (Bjorkoy *et al*., 2005; Kirkin *et al*., 2009; Ichimura and Komatsu, 2010).

Neuronal activation of autophagy can result from upregulation of the autophagic protein 6/beclin-1 (Atg6/beclin-1) or inhibition of the mammalian target of rapamycin. Beclin-1 is an evolutionarily conserved protein that is essential for the nucleation step of autophagy, via its interaction with the class III phosphatidylinositol-3-kinase/Vps34 complex (Zeng *et al*., 2006). Beclin-1 is described to be a crucial and limiting protein for the autophagy pathway. Inactivation of the *Caenorhabditis elegans* beclin-1 gene causes apoptosis (Takacs-Vellai *et al*., 2005) and increases aggregation and neurodegeneration upon mutant huntingtin expression (Jia *et al*., 2007). Furthermore, deletion of one of the beclin-1 alleles in mice is sufficient to cause impaired autophagy and neurodegeneration (Pickford *et al*., 2008). A decrease in beclin-1 levels has been observed in aged brains and in Alzheimer's and Huntington's diseases (Shibata *et al*., 2006; Pickford *et al*., 2008) while its overexpression has been reported to reduce aggregation and improve neuronal function (Pickford *et al*., 2008; Spencer *et al*., 2009). No data are available regarding beclin-1 levels and modelling in Machado–Joseph's disease. Therefore, it is crucial to investigate if the autophagy pathway is impaired in Machado–Joseph disease and if soluble and aggregated forms of mutant ataxin-3 can be selectively degraded by this pathway.

In the present study, we evaluated alterations in the molecular components of autophagy in tissue from patients with Machado–Joseph disease and *in vitro* and *in vivo* models of the disease. We found accumulation of proteins related with the autophagy pathway and autophagosomes in brains of patients with Machado–Joseph disease, as well as decreased beclin-1 levels in tissue from patients with Machado–Joseph disease and rodent models. Furthermore, mutant ataxin-3 aggregates were shown to be recognized by the autophagic receptor p62 while beclin-1 overexpression improved autophagosomal flux, mutant ataxin-3 clearance and neuronal function. Our data provide evidence that the autophagy pathway is altered in the brain of patients with Machado–Joseph disease and that beclin-1 overexpression is able to stimulate the autophagic flux, leading to a selective clearance of mutant ataxin-3.

Materials and methods

Human brain tissue

Post-mortem putamen tissue from three patients with clinically and genetically confirmed Machado–Joseph disease (Patient 1: 62 years, 26/70 CAG repeats; Patient 2: 53 years, 23/69 CAG repeats; Patient 3: 62 years, 22/74 CAG repeats) and midfrontal cortical tissue (69 years, onset at 56) were obtained from the 'Tissue Donation Programme of the National Ataxia Foundation, Minneapolis, MN, USA' (VA Medical Centre, Albany, NY, USA). Controls with no evidence of neurological disease (Control 1: 55 years; Control 2: 56 years; Control 3: 67 years) were obtained from Neurology and Pathology Services of University Hospital of Coimbra, Portugal. The tissue was fresh when dissected, placed in 10% neutral buffered formalin and kept at 4°C.

Transgenic mice tissue

Brains of homozygous transgenic mice ($n = 6$), 10–13 weeks old (late stage of disease), expressing human full-length mutant ataxin-3 with 71 glutamines (Q71-C mice) (Goti *et al*., 2004) and wild-type C57BL/6 mice age matched ($n = 6$) were dissected fresh and kept at –80°C. Small punches of the striatum were collected with a Harris Uni-Core pen, with 2.0 mm diameter (Ted Pella, Inc).

Lentiviral vectors

The complementary DNAs encoding for human *beclin-1* (Liang *et al*., 1999) and rat *light chain 3* (Kabeya *et al*., 2000) fused to the enhanced green fluorescent protein were inserted downstream from the mouse phosphoglycerate kinase 1 promoter in a self-inactivating lentiviral transfer vector (Deglon *et al*., 2000). Viral vectors encoding for the human beclin-1, enhanced green fluorescent protein-light chain 3, human full-length wild-type ataxin-3 with 27 glutamines (Alves *et al*., 2008*b*) and human full length mutant ataxin-3 with 72 glutamines (Alves *et al*., 2008*b*), were produced in human embryonic kidney 293 T cells using a four-plasmid system described previously (de Almeida *et al*., 2002).

In vivo experiments

Adult male Wistar rats (Charles River Laboratories, Inc.), weighing 200–220 g were used. The animals were housed in a temperature-controlled room and maintained on a 12 h light/dark cycle. Food and water were available *ad libitum*. The experiments were carried out in accordance with the European Community Council directive (86/609/EEC) for the care and use of laboratory animals. For the stereotaxic injection of lentiviral vectors, concentrated viral stocks were thawed on ice and resuspended by vortexing. The rats were anaesthetized with ketamine (75 mg/kg intraperitoneally) and xylazine (10 mg/kg intraperitoneally). Particle content of lentiviral vectors was matched to 200 μg of p24/ml. The surgical procedure was performed as described previously (Alves *et al*., 2008*b*). The animals received a single injection of lentivirus in each hemisphere at the following co-ordinates: 0.7 mm rostral to bregma, 3.0 mm lateral to midline and 5.5 mm ventral from the skull surface, with the mouth bar set at 0.0 mm. In all experiments ipsilateral was compared to contralateral hemisphere and only experiments performed with the same batches of virus were compared.

Human fibroblasts culture

Human fibroblast cells were obtained from Coriell cell repositories and skin biopsy (control: 38 years, not affected; Machado–Joseph disease 1: 38 years, 74 CAG repeats; Machado–Joseph disease 2: 28 years, 82 CAG repeats). Cells were kept in culture in Dulbecco's modified Eagle's medium supplemented with 10% bovine serum, 1% non-essential amino acids, 2 mM L-glutamine, 100 U/ml penicillin and 100 μg/ml streptomycin (Gibco) at 37°C in 5% CO_2/air atmosphere.

Striatal primary cells culture

Timed-pregnant Sprague–Dawley rats (Charles Rivers Laboratories) were killed by CO_2 inhalation, and embryos (Embryonic Day 15) were collected in a Petri dish and placed on ice. Dissections were performed under a stereomicroscope and ganglionic eminences were isolated. Culture and infection protocol was performed as described elsewhere (Zala *et al*., 2005). Analysis was performed at 2 weeks post-infection (18 days *in vitro*).

Neuroblastoma cell culture

Mouse neuroblastoma cell line (Neuro-2 a cells) obtained from the American Type Culture Collection cell biology bank (CCL-131) were incubated in Dulbecco's modified Eagle's medium supplemented with 10% foetal bovine serum, 100 U/ml penicillin and 100 μg/ml streptomycin (Gibco) (complete medium) at 37°C in 5%CO_2/air atmosphere. Cells were plated and lipofectamine transfected or infected with lentiviral particles expressing enhanced green fluorescent protein-light chain 3 or ataxin-3 and beclin-1/control, at the ratio of 10 ng of p24 antigen/10^5 cells 24 and 48 h after plating. At 2 weeks post-infection, cells were either lysed for western blot processing or lipofectamine transfected for the flow cytometry experiments.

Antibodies for immunohistochemistry and western blotting

The following primary antibodies were used: mouse monoclonal anti-ataxin-3 (1H9, Chemicon; 1:5000; overnight, 4°C); rabbit polyclonal anti-p62 antibody (Abgent; 1:50; overnight-48 h, 4°C); rabbit polyclonal anti-Atg16L antibody (Abgent; 1:50; overnight-48 h, 4°C); rabbit polyclonal anti-light chain 3 antibody (Abgent; 1:50; overnight-48 h, 4°C); rabbit polyclonal anti-ubiquitin (Dakocytomation; 1:1000; overnight 4°C); mouse monoclonal anti-beclin-1 (BD Biosciences; 1:1000; overnight, 4°C); mouse monoclonal anti-β-actin antibody (1:5000, Sigma); rabbit polyclonal anti-dopamine-and-cyclic Adenosine 5′-monophosphate-regulated phosphoprotein of 32 kDa (DARPP-32) (Chemicon; 1:5000, overnight 4°C); mouse monoclonal anti-neuronal nuclei protein antibody (Chemicon; 1:1000; overnight 4°C).

Histological processing

The human brain tissue was fresh when dissected and placed in cold 10% neutral buffered formalin fixative solution. Rats were killed by sodium pentobarbital overdose, transcardially perfused with 0.1 M phosphate buffer solution and a 4% paraformaldehyde fixative solution (Fluka, Sigma) followed by brain removal. Both tissues were cryoprotected in 25% sucrose-0.1 M phosphate buffer solution solution for 48 h, dry ice-frozen and cut on a cryostat-microtome (Leica CM3050S) in 25–30 μm coronal sections. Slices were collected and stored in 48-well trays (Corning Inc.), free-floating in 0.1 M phosphate buffer solution supplemented with 0.12 μmol/l sodium azide. The plates were stored at 4°C until immunohistochemical processing.

Immunohistochemistry

The immunohistochemical procedure was initiated by incubating brain sections in phenylhydrazine diluted in phosphate buffer solution (1:1000; 15 min, 37°C; light imaging only), followed by a Tris-buffered saline pH 9 antigen retrieval method (30 min, 95°C, human tissue only), blocking in 10% normal goat serum in 0.1% Triton X-phosphate buffered solution (1 h, room temperature) and incubation with the respective primary and secondary antibodies diluted in blocking solution. For light imaging, the secondary antibody used was biotinylated and followed a reaction with the Vectastain elite avidin-biotin-peroxidase kit and by 3,3′-diaminobenzidine substrate (both from Vector Laboratories). Premounted sections were then counterstained with cresyl violet (2 min in cresyl violet solution followed by differentiation in ethanol 70%) or directly dehydrated in toluene and coverslipped with Eukitt mounting medium (O. Kindler GmbH and Co.). Light images were acquired with a Zeiss Axiovert 200 imaging microscope. For the fluorescent imaging, the secondary antibody used was coupled to a fluorophore (Alexa Fluor, Invitrogen) and followed a nuclei staining reaction with 4′,6-diamino-2-phenylindole (5 min, room temperature). Images were acquired with a confocal LSM Zeiss. All immunohistochemical analyses were performed in triplicate and using at least three sections of each experimental set.

Immunohistochemistry quantitative analysis

The human brain tissue analysis for the p62-, Atg16L- and light chain 3-positive cells were carried out counting for each staining, 10 fields (×100 magnification) of three different sections. Only cytoplasmic puncta-like immunoreactivity was scored positive. For each field and staining, normalization was relative to total number of nuclei (cresyl staining).

The quantitative analysis of enhanced green fluorescent protein-light chain 3 positive puncta was carried out counting eight fields (×100 magnification) of three different brain sections from four animals

sacrificed at 12 weeks post-injection ($n = 4$). Hemispheres injected with mutant ataxin-3 and wild-type ataxin-3 were counted and only cytoplasmic puncta-like immunoreactivity was scored positive. For each field, normalization was relative to total number of nuclei (4′,6-diamino-2-phenylindole staining).

The quantification of ataxin-3 and ubiquitin-positive inclusions was performed by scanning 8–10 coronal sections spread over the anterior–posterior extent of the striatum (inter-section distance: 200 μm), using a ×10 objective on a Zeiss Axioplan2 Imaging microscope motorized for *x*, *y* and *z* displacements, and an image acquisition and analysis software (Mercator, Explora Nova). For each animal, the absolute number of inclusions in the striatum was calculated as described previously (Alves *et al*., 2008*a*) . For the quantification of DARPP-32 and neuronal nuclei protein depleted volumes, scanning of 8–10 coronal sections spread over the anterior–posterior extent of the striatum (inter-section distance: 200 μm), using a MCID^{TM} acquisition and software analysis apparatus was performed. The volume was estimated as described elsewhere (Alves *et al*., 2008*a*) and data were expressed as the evaluated DARPP-32 or neuronal nuclei protein depleted volume (mm^3).

Protein extraction and western blotting

For the protein extraction protocol, brain tissue and cells were lysed in radioimmunoprecipitation assay-buffer solution (50 mM Tris HCl, pH 8, 150 mM NaCl, 1% NP-40, 0.5% sodium deoxycholate, 0.1% sodium dodecyl sulphate) containing proteases inhibitors (Roche diagnostics GmbH) followed by a 4 s ultra-sound chase (1 pulse/s). Total protein lysates were stored at –80°C and protein concentration was determined with the Bradford protein assay (BioRad). Depending on the analysis, 20 (Neuro-2 a), 30 (transgenic mice brains and striatal primary cells) and 60 (human fibroblasts) μg of protein extract were resolved in sodium dodecyl sulphate-polyacrylamide gels (4% stacking, 12% running; 20–80%) with exception of striatal primary cells analysis that were resolved in different sodium dodecyl sulphate-polyacrylamide gels (4% stacking, 6% running; 50–50%). The proteins were transferred onto polyvinylidene difluoride membranes (GE Healthcare) according to standard protocols. The immunobloting procedure was performed as described previously (Alves *et al*., 2008*a*) with the respective primary antibodies, followed by incubation with the respective alkaline phosphatase-linked secondary antibody. Bands were visualized with Enhanced Chemifluorescence substrate (ECF) (GE Healthcare) and chemifluorescence imaging (VersaDoc Imaging System Model 3000, Bio-Rad). The western blot analyses were performed at least in triplicate for each experimental set. Membranes were stripped using a 0.1 M glycine pH 2.3 (30 min, room temperature) and reprobed with mouse monoclonal anti-β-actin antibody (1:5000, Sigma). Densitometric analysis was carried out using ImageJ software (NIH).

Flow cytometry analysis

For the transient transfection experiments, Neuro-2 a cells were plated and transfected with lipofectamine (Invitrogen) 24 h after plating. Lipofectamine was used according to the manufacturer's protocol, and cells transfected with enhanced green fluorescent protein-light chain 3 with wild-type or mutant ataxin-3 plus beclin-1 or cytoplasmic LacZ as control (1:1:1 DNA ratio). After 24, 48, 72 and 96 h post-transfection, cells were harvested with trypsin/ethylenediaminetetraacetic acid (Gibco), washed and resuspended in 0.5–1.0 ml of complete medium without phenol red for fluorescence activated cell sorter analysis. For the stable enhanced green fluorescent protein-light chain 3 expression analysis, cells were plated, infected with enhanced green fluorescent protein-light chain 3 lentiviral particles and transfected with lipofectamine for the ataxin-3 and beclin-1/control constructs (1 : 1 DNA ratio) at 2 weeks post-infection. The analysis was performed 48 h post-transfection. For the starvation conditions, cells were incubated for 3 h with Hanks buffer saline solution modified to have 1.8 g/l of glucose (Sigma). For all conditions, cells were harvested with trypsin/ethylenediaminetetraacetic acid (Gibco), washed and resuspended in 0.5–1.0 ml of Hanks buffer saline solution for fluorescence activated cell sorter analysis. Samples were kept on ice until use and analysis of 50 000 viable cells per sample was performed on a fluorescence activated cell sorting flow cytometer (Becton Dickinson), where the data of viable cell counts was plotted as enhanced green fluorescent protein fluorescence intensity (Fl1 channel, 530 ± 30 nm). The flow cytometry analysis was performed in triplicate for each experimental set.

Results

Molecular components of the autophagy pathway abnormally accumulate in Machado–Joseph disease brain tissue

An abnormal number of autophagosomes within cells has been reported as a hallmark of altered autophagy in the brain (Kegel *et al*., 2000; Nixon *et al*., 2005). For this reason, we investigated if components of the autophagy pathway were abnormally accumulating in post-mortem brain tissue of patients with Machado–Joseph disease. The immunoreactivity for autophagy components in an affected brain area—the putamen—of three autopsy-confirmed patients with Machado–Joseph disease (Patients 1–3, Fig. 1) was compared to three age-matched controls (Controls 1–3, Fig. 1) and an unaffected brain area, midfrontal cortex, of an autopsy-confirmed patient with Machado–Joseph disease (Fig. 1).

We found high immunoreactivity for mutant ataxin-3 aggregates (Fig. 1A) and for components involved in sequential steps of the autophagy pathway (Fig. 1B–E) in the putamen of patients with Machado–Joseph disease but not in controls. A strong nuclear and cytoplasmic puncta-like immunoreactivity for the sequestosome 1/p62 protein (Fig. 1B) was observed in the putamen of patients with Machado–Joseph disease but not in controls ($n = 3$, Fig. 1E; 38.51 ± 0.21 versus 10.20 ± 3.85 in controls; $P = 0.0029$). This protein binds ubiquitinated proteins, redirects them to autophagosomes and interacts with the light chain 3-II protein, before being degraded with other cellular components (Bjorkoy *et al*., 2005; Kirkin *et al*., 2009; Ichimura and Komatsu, 2010). A robust cytoplasmic puncta-like immunoreactivity was also observed for the autophagic protein 16, (Atg16L) protein (Fig. 1C), which integrates the Atg12-Atg5-Atg16L complex, in the putamen of patients with Machado–Joseph disease but not in controls ($n = 3$, Fig. 1E; 44.79 ± 1.42 versus 8.75 ± 3.05 in controls; $P = 0.0004$). This complex is important for the lipidation of light chain 3 and is present in the autophagosomal membrane during the elongation phase, being a marker of immature autophagosomes (Ichimura and Komatsu, 2010). Finally, we analysed

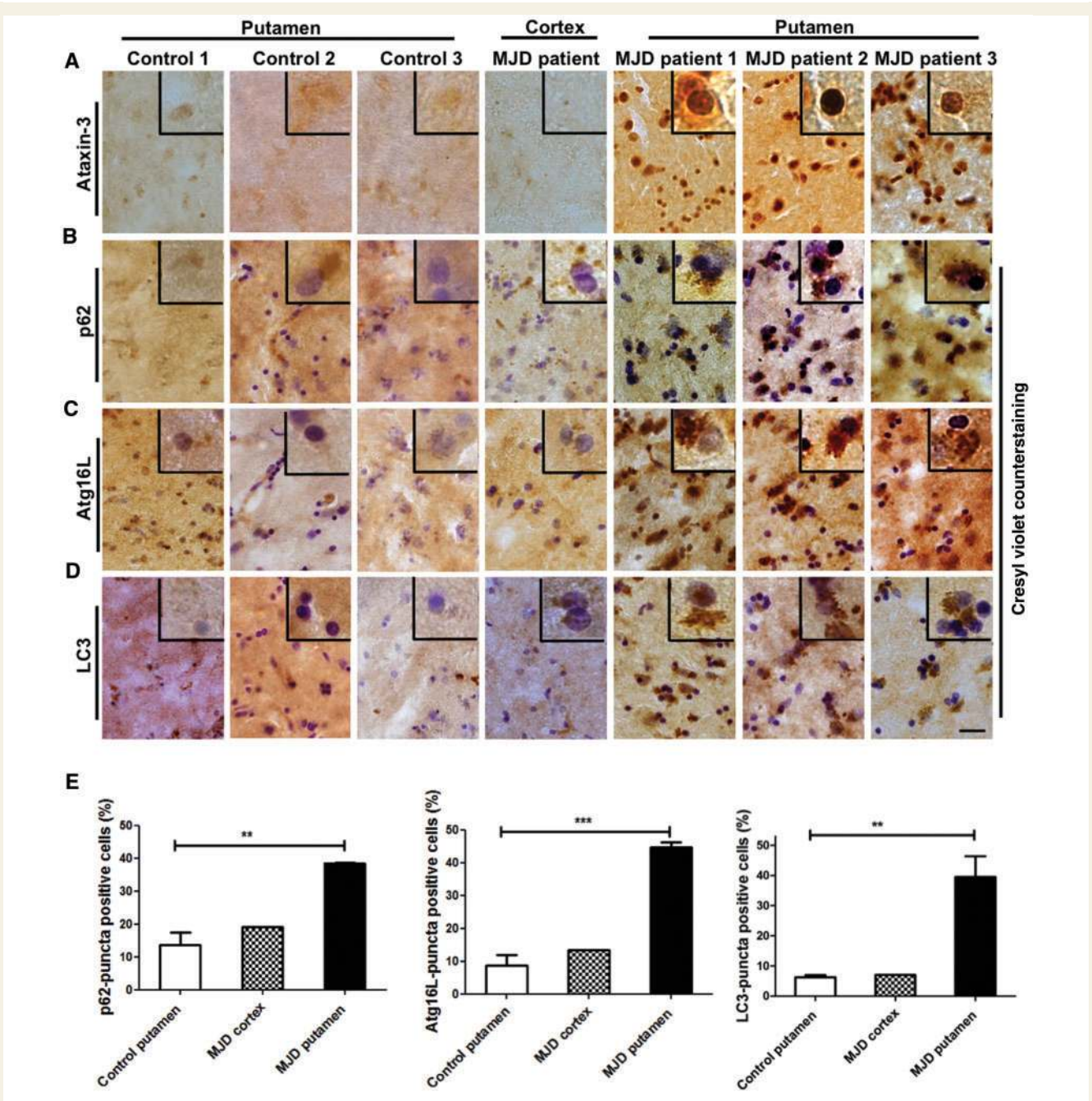

Figure 1 The autophagy pathway is impaired in brain tissue of patients with Machado–Joseph disease. (**A–D**) Immunohistochemical analysis of midfrontal cortex and putamen of cortex and putamen of postmortem brain samples of Machado–Joseph disease patients (MJD; $n = 3$) and age-matched controls (control, $n = 3$). (**A**) Representative brain sections stained for ataxin-3 to highlight mutant ataxin-3 aggregates in the putamen of patients with Machado–Joseph disease. (**B**) Representative brain sections stained for the autophagic receptor p62 counterstained with cresyl violet. (**C**) Representative brain sections stained for the autophagic protein Atg16L counterstained with cresyl violet. (**D**) Representative brain sections stained for the autophagosomal marker light chain 3 (LC3) counterstained with cresyl violet. (**E**) Quantitative analysis of the strong cytoplasmic puncta-like immunoreactivity for the p62 (left), Atg16L (middle) and light chain 3 (right) observed in the putamen of patients with Machado–Joseph disease but not in controls. Normalization was performed to total cell number (cresyl violet counterstaining). Results are expressed as the percentage ratio of puncta-positive cells/total cells. Values correspond to mean ± standard error of the mean. $^{**}P < 0.01$; $^{***}P < 0.001$ (unpaired Student's *t*-test). Scale bar: 20 μm.

the microtubule-associated protein 1 light chain 3 (LC3) (Fig. 1D). This protein is an essential component of the autophagosomal membrane and a marker of all autophagosomal structures, immature and mature autophagosomes, as well as autophagolysosomes. A clear cytoplasmic-puncta-like immunoreactivity was observed in the putamen of patients with Machado–Joseph disease but not in controls ($n = 3$, Fig. 1E; 41.01 ± 5.69 versus 6.25 ± 0.72 in controls; $P = 0.003$).

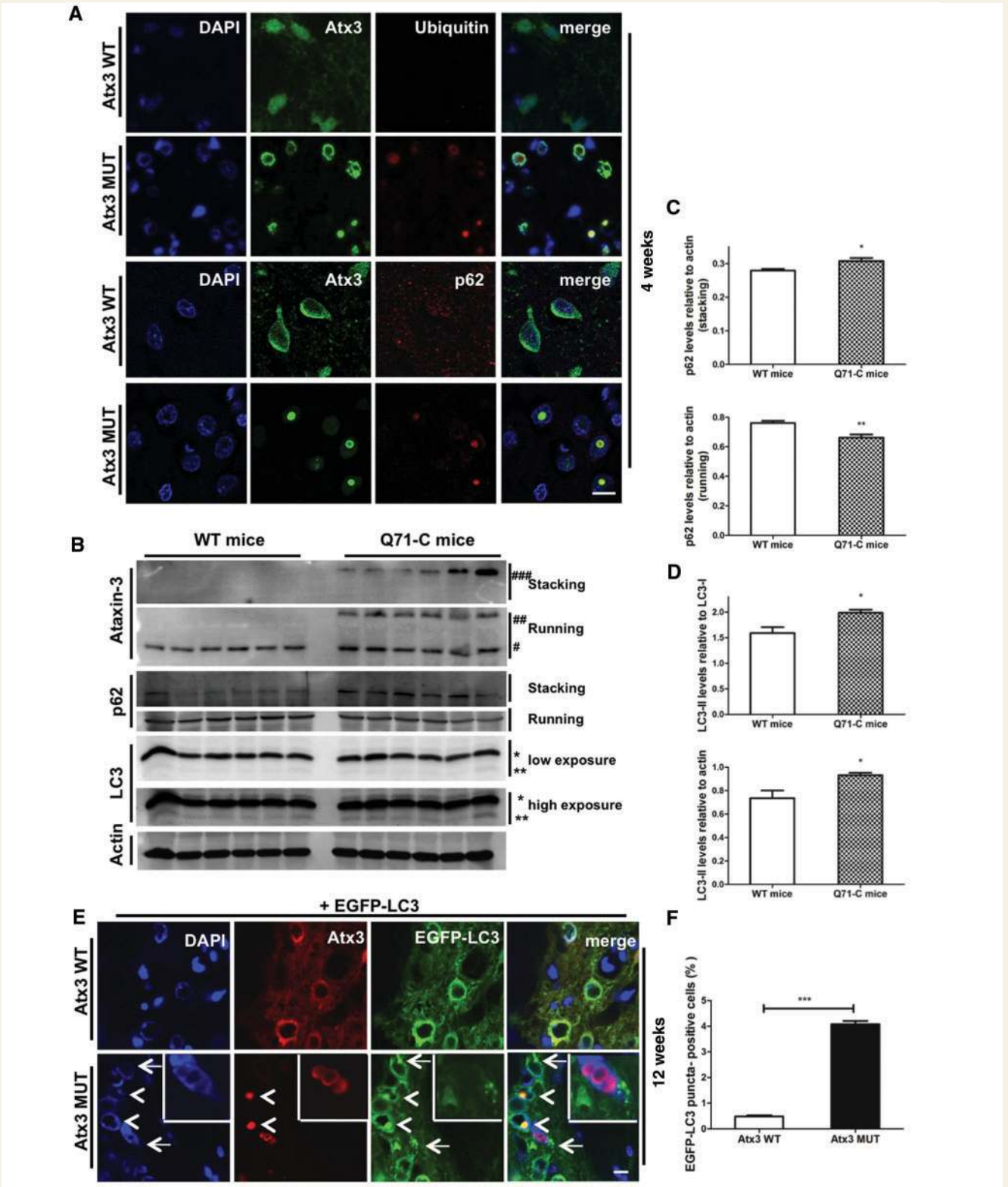

Figure 2 Early activation of the p62 autophagic receptor and late accumulation of autophagosomes. (**A**) Laser confocal microscopy analysis of rat striatal sections upon mutant (Atx3 MUT) and wild-type (Atx3 WT) ataxin-3 expression. The analysis was performed at 4 weeks post-injection ($n = 4$) by staining for nuclei (4′,6-diamidino-2-phenylindole, blue), ataxin-3 (green), ubiquitin (red, upper) and p62 (red, lower). (**B–D**) Western blot analysis of lysates of striatal brain punches of late stage Machado–Joseph disease transgenic mice expressing human mutant ataxin-3 with 71 glutamines (Q71-C mice, $n = 6$) and age-matched wild-type C57BL/6 mice (wild-type mice, $n = 6$), used as control. (**B**) Representative western blot probed with ataxin-3, p62, light chain 3 (LC3) and actin antibodies. Insoluble proteins with a molecular weight superior to 250 kDa accumulate in the stacking gel (4% acrylamide), whereas soluble proteins with a

(continued)

These data suggest impairment of the autophagic pathway, since autophagosomes are efficiently cleared in the central nervous system (Boland *et al*., 2008) and accumulation of p62 and light chain 3-positive autophagosomes has been associated with impairment in the trafficking to lysosomes and protein degradation (Bjorkoy *et al*., 2005; Komatsu *et al*., 2007; Pankiv *et al*., 2007).

Early activation of the p62 autophagic receptor and late accumulation of light chain 3-positive autophagosomes

Autophagy has been described as an essential cellular mechanism for the clearance of ubiquitin-positive inclusions (Hara *et al*., 2006; Komatsu *et al*., 2006). Recently, p62/SQSTM1 was identified as an important constituent of ubiquitinated protein aggregates, allowing its selective degradation through the autophagy pathway (Bjorkoy *et al*., 2005; Pankiv *et al*., 2007). Therefore, to investigate whether mutant ataxin-3 inclusions were targeted for autophagy-mediated degradation, ubiquitin (Fig. 2A, upper panel) and p62 (Fig. 2A, lower panel), immunostaining was performed in rats injected with mutant ataxin-3 or wild-type ataxin-3 at 4 ($n = 4$, Fig. 2A) and 8 weeks ($n = 4$, data not shown) post-injection. At 4 weeks, mutant ataxin-3 inclusions had already co-localized with ubiquitin in the nucleus. Importantly, the cytoplasmic autophagic receptor p62 was found translocated to the nucleus and co-localizing with ubiquitinated mutant ataxin-3 inclusions (Fig. 2A, lower panel).

In addition, western blot analysis of striatal samples from late stage Machado–Joseph disease transgenic mice (Goti *et al*., 2004) (Q71-C mice, $n = 6$, Fig. 2B–D) and age-matched wild-type animals (wild-type mice, $n = 6$, Fig. 2B–D) revealed that p62-positive aggregates (stacking gel, molecular weight >250 kDa) were significantly increased in Q71-C mice ($n = 6$, Fig. 2C; 0.31 ± 0.009) when compared to controls (wild-type mice, $n = 6$, Fig. 2C; 0.28 ± 0.005; $P = 0.019$). This increase of p62 aggregated form was accompanied by a significant reduction in p62 soluble levels (running gel, molecular weight: 50 kDa; $n = 6$, Fig. 2C; 0.66 ± 0.020 versus 0.76 ± 0.014 in controls; $P = 0.003$) as well as an increase of light chain 3-II autophagosomal marker ($n = 6$, Fig. 2D; 1.99 ± 0.061 versus 1.59 ± 0.12 in controls; $P = 0.014$ relative to light chain 3-I; 0.93 ± 0.021 versus 0.74 ± 0.066 in controls; $P = 0.017$ relative to actin). To further assess autophagosomal trafficking in Machado–Joseph disease, we cloned the autophagosomal marker enhanced green fluorescent protein-light chain 3 in the lentiviral vector (Supplementary Fig. 1C, E). This vector was co-injected with the mutant or wild-type ataxin-3-expressing lentiviral vectors in the rat brain. Histochemical analyses were performed at 1 ($n = 2$, data not shown), 4 ($n = 7$, data not shown), 8 ($n = 7$, data not shown) and 12 weeks post-injection ($n = 4$, Fig. 2E and F) by staining for nuclei (4′,6-diamidino-2-phenylindole, blue), ataxin-3 (red) and direct visualization of enhanced green fluorescent protein (light chain 3, green). Cytoplasmic autophagosomal accumulation (arrows) was observed only at 12 weeks post-injection (Fig. 2E and F), a late stage of disease in this model, in a small but highly significant number of cells expressing mutant ataxin-3 ($n = 4$, Fig. 2F; 4.08 ± 0.13), while almost no accumulation was observed upon wild-type ataxin-3 expression ($n = 4$, Fig. 2F; 0.48 ± 0.044; $P = 0.0007$). A high co-localization of light chain 3 protein with perinuclear ataxin-3 aggregates was also found, starting at 4 weeks (data not shown) up to 12 weeks (Fig. 2E, arrow heads). Quantitative real-time polymerase chain reaction confirmed that wild-type and mutant ataxin-3 s were expressed at similar levels (Supplementary Fig 2C).

Altogether, these results suggest that ubiquitinated ataxin-3 inclusions are recognized by the autophagic receptor p62 and therefore by the autophagic machinery in an early stage of disease. Moreover, impairments in this pathway are apparent at late stages of disease, possibly due to saturation in the degradative capacity of the autophagic machinery to clear mutant proteins.

Figure 2 Continued
molecular weight equal or inferior to 250 kDa enter the running gel (12% acrylamide). Note the presence of mutant ataxin-3 aggregates in the stacking gel (###, molecular weight >250 kDa), whereas mutant soluble (##, molecular weight: 66 kDa) and endogenous murine ataxin-3 (#, molecular weight: 46 kDa) were present in the running gel. Note in addition, the p62 protein in the stacking gel (molecular weight >250 kDa) and in the soluble fraction (molecular weight: 50 kDa) and also the autophagosomal membrane marker, light chain 3-II (**, molecular weight: 14 kDa) and its cytoplasmic isoform, light chain 3-I (*, molecular weight: 17 kDa). Actin staining (molecular weight: 42 kDa) was used as loading control. (**C–D**) Optical densitometry analysis. (**C**) The p62 levels present in the stacking gel (upper) and running gel (lower) were normalized according to the amount loaded (actin). Results are expressed as ratio p62/actin. Values are expressed as mean ± standard error of the mean. $*P < 0.05$; $**P < 0.01$ (unpaired Student's *t*-test). (**D**) The light chain 3-II levels were normalized according to the amount of its precursor protein (LC3-I, upper) and amount loaded (actin, lower). Results are expressed as ratio light chain 3-II/light chain 3-I and light chain 3-II/actin. Values are expressed as mean ± standard error of the mean. $*P < 0.05$; $**P < 0.01$ (unpaired Student's *t*-test). (**E** and **F**) *In vivo* enhanced green fluorescent protein-light chain 3 analysis. (**E**) Laser confocal microscopy analysis of rat striatal sections upon mutant and wild-type ataxin-3 co-expression with the autophagosomal marker vector fused to enhanced green fluorescent protein, enhanced green fluorescent protein-light chain 3. Nuclei (4′,6-diamidino-2-phenylindole, blue), ataxin-3 (red) and enhanced green fluorescent protein-light chain 3 (green) are highlighted. At 12 weeks post-injection ($n = 4$), autophagosomal accumulation (autophagosomal puncta, arrows) was observed in rats expressing mutant ataxin-3, while no accumulation was observed upon wild-type ataxin-3 expression. Enhanced green fluorescent protein-light chain 3 was also associated with perinuclear mutant ataxin-3 aggregates (arrow heads). (**F**) Quantification of autophagosomal-positive cells. Results are expressed as the percentage ratio enhanced green fluorescent protein-light chain 3 puncta-positive cells/total cells. Values are expressed as mean ± standard error of the mean. $***P < 0.001$ (paired Student's *t*-test). DAPI = 4′,6-diamidino-2-phenylindole. Scale bar: **A** = 10 μm; **E** = 10 μm.

Levels of the autophagic protein beclin-1 are reduced in fibroblasts from patients with Machado–Joseph disease and rodent models

To further investigate the basis of the late stage-autophagy impairment, we evaluated beclin-1 endogenous levels in a late stage Machado–Joseph disease transgenic mouse model ($n = 6$, Fig. 3A and B), in fibroblasts derived from patients with Machado–Joseph disease ($n = 2$, Fig. 3C and D) and in the Machado–Joseph disease rat model at 1 ($n = 2$, data not shown), 4 ($n = 4$, data not shown) and 8 weeks post-injection ($n = 4$, Fig. 3E). Beclin-1 levels were significantly decreased in transgenic mutant ataxin-3 mice (Q71-C mice, $n = 6$, Fig. 3A and B; 0.89 ± 0.011) compared to control (wild-type mice, $n = 6$, Fig. 3A and B; 1.053 ± 0.026; $P = 0.0002$). In addition, beclin-1 levels were also significantly reduced in fibroblasts from patients with Machado–Joseph disease (Fig. 3C and D; control: 1.15 ± 0.038; Machado–Joseph disease 1: 0.86 ± 0.087; Machado–Joseph disease 2: 0.69 ± 0.05; $^{*}P < 0.05$; $^{**}P < 0.01$). In the lentiviral-based Machado–Joseph disease rat, beclin-1 was trapped in nuclear mutant ataxin-3 inclusions at 8 weeks post-injection (Fig. 3E), while in controls (wild-type ataxin-3 expression; Fig. 3E) beclin-1 had a widespread cytoplasmic distribution within the cell. This could indicate that along with the progression of the disease, beclin-1 becomes trapped in the insoluble mutant ataxin-3 inclusions, while its soluble and functional levels progressively decrease. These data suggest that reduced levels of beclin-1 protein are present in Machado–Joseph disease pathogenesis and may contribute to the late-stage associated impairment of autophagy and progression of the disease.

Beclin-1 overexpression improves clearance of aggregated, oligomeric and soluble mutant ataxin-3

These data prompted us to investigate whether the upregulation of the autophagy pathway, through increase in the levels of beclin-1, could improve mutant ataxin-3 clearance and delay the development of neuropathology. For that purpose, we co-expressed human beclin-1 (Supplementary Fig. 1) and mutant ataxin-3 in primary striatal cells (Supplementary Fig. 2) and in the rat model. Western blot analysis of primary striatal cells infected with lentiviral vectors expressing wild-type ataxin-3 and mutant ataxin-3 alone and co-infected with human beclin-1 at 2 weeks post-infection showed three different species of ataxin-3: (i) insoluble aggregates; (ii) soluble oligomers; and (iii) soluble mutant and wild-type ataxin-3. Strikingly, radioimmunoprecipitation assay buffer-insoluble ataxin-3 aggregates (stacking gel, molecular weight >250 kDa) were only visible in samples containing mutant ataxin-3 (Fig. 4A) and not in samples co-expressing mutant ataxin-3 and beclin-1 (Fig. 4A). Optical densitometry analysis of the membrane (Fig. 4C) revealed a drastic reduction of aggregated ataxin-3 in beclin-1-treated (0.074 ± 0.0034) as compared to non-treated mutant ataxin-3 cells (0.75 ± 0.18; $P = 0.0039$). A similar decrease of ataxin-3 oligomers (stacking-running gel interface, #, molecular weight: 250 kDa) (Fig. 4A and C) in beclin-1 treated (0.079 ± 0.0050) compared to non-treated samples (0.86 ± 0.23; $P = 0.0065$) was observed. Finally, beclin-1 led to a significant decrease of radioimmunoprecipitation assay buffer soluble mutant ataxin-3 (running gel, molecular weight: 64 kDa; Fig. 4A and C; 0.85 ± 0.036 versus 2.85 ± 0.65 in control; $P = 0.012$). Non-overexposed membranes were used for quantification (Supplementary Fig. 2B). Probing of the membranes with an ubiquitin antibody (Fig. 4B) and quantification (Fig. 4D) revealed the presence of ubiquitin-positive aggregates in the stacking fraction of the gel (top to #; 2.68 ± 0.40) that were reduced in cells co-expressing beclin-1 (0.41 ± 0.032; $P = 0.0002$).

In the Machado–Joseph disease rat model (Fig. 4E–H), immunohistochemistry and quantitative analysis for ataxin-3 and ubiquitin-positive inclusions (Fig. 4F–H) revealed a significant beclin-1-mediated reduction at 4 weeks in the number of ataxin-3 inclusions ($n = 8$, Fig. 4F; Fig. 4G left; $121\,683 \pm 21\,341$ versus $185\,866 \pm 32\,343$ inclusions in controls; $P = 0.039$) as well as in the number of ubiquitin inclusions ($n = 8$, Fig. 4F; Fig. 4H left; $52\,629 \pm 7762$ versus $77\,077 \pm 11\,901$ inclusions in controls; $P = 0.042$). This beclin-1-mediated clearance was even more pronounced at 8 weeks post-injection ($n = 8$, Fig. 4F and G; ataxin-3 inclusions $133\,947 \pm 24\,883$ versus $218\,062 \pm 21\,594$ inclusions in controls; $P = 0.0033$) (Fig. 4F and H; ubiquitin inclusions $62\,066 \pm 11\,013$ versus $99\,789 \pm 8891$ inclusions in controls; $P = 0.0006$). Quantitative real-time polymerase chain reaction confirmed that mutant ataxin-3 and mutant ataxin-3 plus Beclin-1 striatal cells express ataxin-3 at similar levels (Supplementary Fig. 2D). Together these findings indicate that beclin-1 was able to clear soluble, oligomeric and aggregated toxic species of ataxin-3 over time.

Beclin-1 overexpression reduces neuronal dysfunction mediated by mutant ataxin-3

In view of these results, we next investigated if clearance of ataxin-3 different species would result in neuroprotective effects. Given that lentiviral expression of mutant ataxin-3 produces a depletion of neuronal DARPP-32 marker and neuronal nuclei protein that can be precisely quantified (Alves *et al.*, 2008*a*), immunohistochemistry for DARPP-32 (Fig. 5A) and neuronal nuclei protein (Fig. 5A) was performed. Beclin-1 overexpression led to a significant reduction of neuronal dysfunction as revealed by the decrease at 4 weeks (Fig. 5B and C) of DARPP-32 ($n = 8$, Fig. 5B; 1.25 ± 0.17 versus $1.94 \pm 0.29\,mm^3$ in controls; $P = 0.0019$) and neuronal nuclei protein-depleted volumes ($n = 8$, Fig. 5C; 0.80 ± 0.11 versus $1.63 \pm 0.30\,mm^3$ in controls; $P = 0.0092$). Importantly, this protective effect was conserved at 8 weeks post-injection as revealed by DARPP-32 ($n = 8$, Fig. 5B; 1.82 ± 0.27 versus $3.14 \pm 0.40\,mm^3$ in controls; $P = 0.0003$) and neuronal nuclei protein immunoreactivity ($n = 8$, Fig. 5D; 1.26 ± 0.16 versus $2.38 \pm 0.11\,mm^3$ in controls; $P = 0.000007$). In addition, beclin-1 overexpression

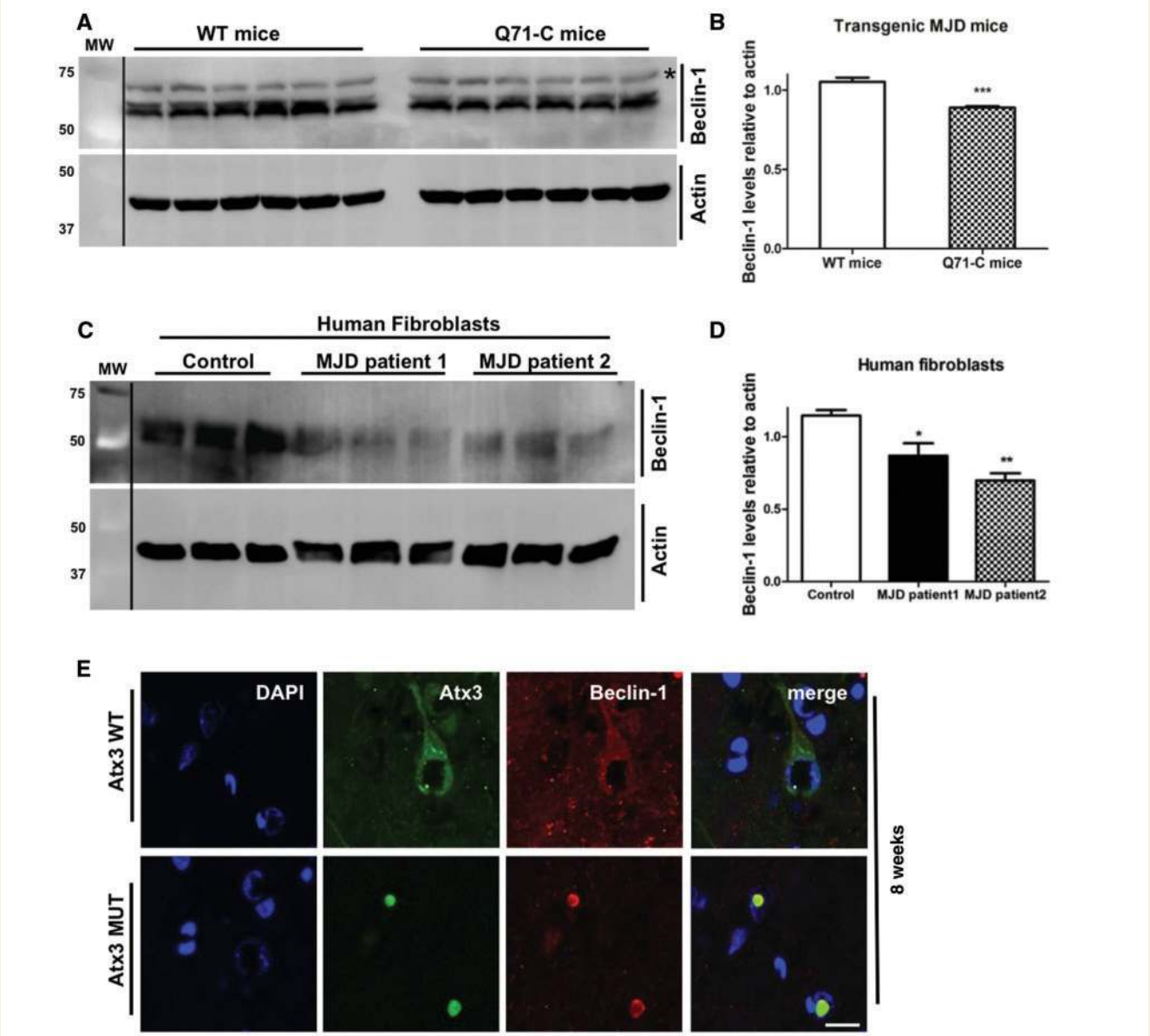

Figure 3 Endogenous beclin-1 is decreased in tissue of patients with Machado–Joseph disease and animal models. (**A** and **B**) Western blot analysis of lysates of striatal brain punches of late stage Machado–Joseph disease (MJD) transgenic mice expressing human mutant ataxin-3 with 71 glutamines, (Q71-C mice, $n = 6$) and age-matched wild-type (WT) C57BL/6 mice (wild-type mice, $n = 6$), used as controls. (**A**) Representative western blot probed for endogenous murine beclin-1 (molecular weight: 52 kDa) and actin (molecular weight: 42 kDa) proteins. (**B**) Optical densitometry analysis. Each beclin-1 lane was normalized according to the actin band. Results are expressed as ratio beclin-1/actin. Values are expressed as mean ± standard error of the mean. $***P < 0.001$ (unpaired Student's *t*-test). (**C** and **D**) Western blot analysis of lysates of human fibroblasts derived from patients with Machado–Joseph disease (Patients 1 and 2) and control individual. (**C**) Representative western blot probed for endogenous human beclin-1 (molecular weight: 52 kDa) and actin (molecular weight: 42 kDa) proteins. (**D**) Optical densitometry analysis. Each beclin-1 lane was normalized according to the actin band. Results are expressed as ratio beclin-1/actin. Values are expressed as mean ± standard error of the mean. $*P < 0.05$; $**P < 0.01$ (one-way ANOVA, Dunnett post-test). (**E**) Laser confocal microscopy analysis of rat striatal sections upon mutant ataxin-3 and wild-type ataxin-3 expression. The analysis was performed at 8 weeks post-injection ($n = 4$), by staining for nuclei (4′,6-diamidino-2-phenylindole, blue), ataxin-3 (green) and beclin-1 (red). Scale bar = 10 μm. Atx3 MUT = mutant ataxin-3; DAPI = 4′,6-diamidino-2-phenylindole; MW = moleclular weight; WT Atx3 = wild-type ataxin-3.

was associated with reduced microglial (Supplementary Fig. 4A; 4 weeks) and astroglial activations (Supplementary Fig. 4A; 8 weeks). Unexpectedly, beclin-1 silencing in the brain of adult wild-type rats expressing mutant ataxin-3 did not aggravate mutant ataxin-3-induced neuropathology (Supplementary Fig. 3). This might be due to an insufficient downregulation of protein levels (67% in primary striatal cultures; Supplementary Figs 2 and 3) which, within the short period of time (8 weeks),

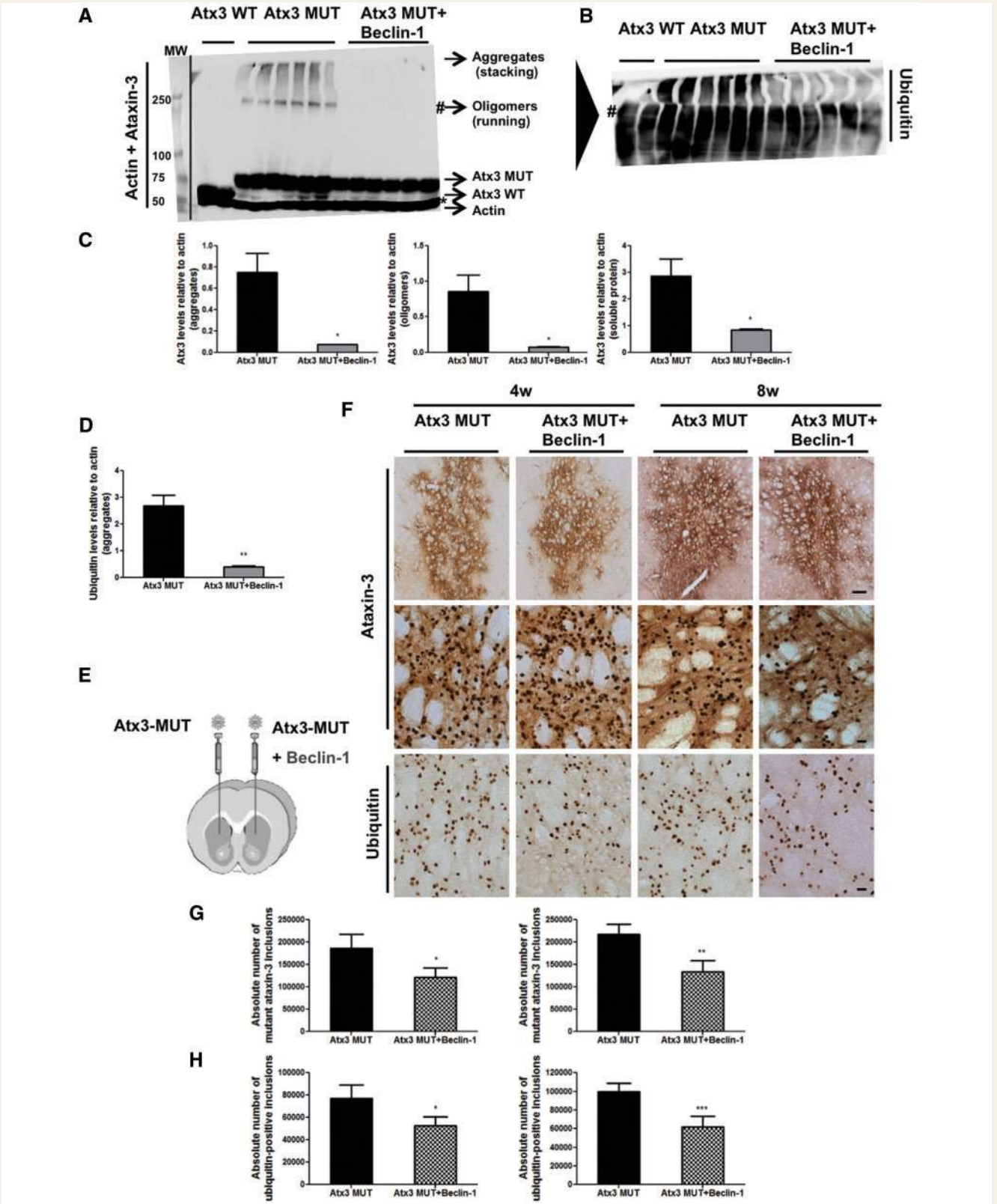

Figure 4 Overexpression of beclin-1 improves clearance of aggregated, oligomeric and soluble mutant ataxin-3. (**A–D**) Analysis of lentiviral-based Machado–Joseph disease (MJD) primary cell culture model. (**A** and **B**) Western blot analysis of rat primary striatal cells lysates. Cells were infected with lentiviral vectors expressing human wild-type and mutant ataxin-3, co-infected with human beclin-1 (Beclin-1) or control. Analyses were performed at 2 weeks post-infection ($n = 6$ for each experimental set). (**A**) Representative western blot loaded in 4–6% acrylamide gel and membrane probed with ataxin-3 and actin antibodies. Note the presence of human wild-type ataxin-3 (molecular weight: 50 kDa), mutant ataxin-3 (molecular weight: 67 kDa), endogenous rat ataxin-3 (*, molecular weight: 48 kDa)

(continued)

failed to produce significant exacerbation of Machado–Joseph disease pathology.

Overall, these results indicate that beclin-1 overexpression mitigates Machado–Joseph disease neuropathology.

Beclin-1 improves autophagosomal flux and ataxin-3 clearance in neuroblastoma cells expressing mutant ataxin-3

To investigate whether beclin-1 effects were mediated through activation of the autophagic pathway, we performed an autophagosomal flux analysis in neuroblastoma cells (Neuro-2 a) transiently (Fig. 6B–E) and stably expressing enhanced green fluorescent protein-light chain 3 (Fig. 6F). The enhanced green fluorescent protein-light chain 3 protein acts similarly to the endogenous light chain 3 and translocates from the cytoplasm (light chain 3-I) to the autophagosomal membrane (light chain 3-II) where it remains until complete fusion to lysosomes (Bampton *et al*., 2005; Fig. 6A, Step 1–2). Once inside the lysosomes, the acidic pH will block the emission of enhanced green fluorescent protein fluorescence (Fig. 6A, Step 3) (Mizushima *et al*., 2010). Therefore, an increase in the autophagosomal flux leads to an increased enhanced green fluorescent protein-light chain 3 degradation, and concomitant reduction of its fluorescence emission (Shvets *et al*., 2008).

For the transient enhanced green fluorescent protein-light chain expression flow cytometry analysis, Neuro2a cells were transiently transfected with enhanced green fluorescent protein-light chain 3 and ataxin-3 in the presence of beclin-1/control vectors. Flow cytometry was performed on live cells 24, 48, 72 and 96 h post-transfection. Enhanced green fluorescent protein-light chain fluorescence emission progressively increased reaching its maximum at 48 h post-transfection. A similar fluorescence pattern was observed between control-treated ataxin-3 wild-type (Fig. 6B, orange) and mutant ataxin-3 (Fig. 6B, blue). In cells co-expressing mutant ataxin-3 and beclin-1 (Fig. 6C, red), the fluorescence intensity of enhanced green fluorescent protein-light chain 3 was significantly lower compared to cells co-expressing mutant ataxin-3 and control cDNA (Fig. 6C, blue) ($n = 3$, Fig. 6C; 48 h: 10.25 ± 0.1 versus 11.65 ± 0.53 in control cDNA, $P < 0.01$; 72 h: 9.60 ± 0.56 versus 11.30 ± 0.28 in control cDNA, $P < 0.001$). Furthermore, the fluorescence intensity was lower in mutant ataxin-3/beclin-1 expressing cells (Fig. 6D, red) as compared to wild-type ataxin-3/beclin-1 cells (Fig. 6D, green) ($n = 3$, Fig. 6D; 48 h: 10.25 ± 0.1 versus 12.78 ± 0.63 in wild-type ataxin-3, $P < 0.001$; 72 h: 9.60 ± 0.11 versus 10.75 ± 0.05 in wild-type ataxin-3, $P < 0.05$), suggesting that the autophagosomal flux of mutant ataxin-3 is more affected by beclin-1 overexpression as compared to the wild-type ataxin-3. The fact that the results obtained with wild-type ataxin-3 /beclin-1 (Fig. 6E, green) or control-treated cells (Fig. 6E, orange) were not significantly different, confirms this interpretation.

In order to confirm these results, the same experiment was performed with cells stably expressing enhanced green fluorescent protein-light chain 3 (Fig. 6F). The flow cytometry analysis was performed 48 h post-transfection of ataxin-3 and beclin-1/control constructs in cells incubated for 3 h in complete medium (full bars) or under starvation conditions (vertical stripes bars). As expected, the fluorescence intensity of cells stably expressing enhanced green fluorescent protein-light chain 3 was higher than cells transiently expressing enhanced green fluorescent protein-light chain 3. In agreement with prior results, under complete medium conditions (Fig. 6F, full bars) beclin-1 led to a selective improvement in the autophagosomal flux of cells expressing mutant ataxin-3 ($n = 3$, Fig. 6F, red; 80.33 ± 0.88 versus 96.60 ± 1.14 in control-treated, blue; $P < 0.001$) but not in cells expressing wild-type ataxin-3 ($n = 3$, Fig. 6F, green; 96.13 ± 2.26 versus 93.80 ± 1.18 in control-treated, orange). The starvation conditions (Fig. 6F, striped bars) led to a robust and significant decrease in the enhanced green fluorescent protein-light chain 3 fluorescence intensity in all experimental sets analysed (decrease from 35.62 to 47.25%; $P < 0.001$). Furthermore, under starvation,

Figure 4 Continued
and actin (molecular weight: 42 kDa). Importantly, in the 4% acrylamide gel fraction (stacking gel, top to #), the presence of ataxin-3 aggregates (molecular weight >250 kDa) and oligomers (250 kDa) was noticeable only in mutant ataxin-3 lanes. Actin staining was used as loading control. (**B**) Membrane represented on (**A**) probed with ubiquitin antibody. (**C** and **D**) Optical densitometry analysis. (**C**) Each ataxin-3 lane was normalized according to the amount loaded (actin). Separate quantification of aggregates (left), oligomers (middle) and soluble mutant protein (right) was performed. Short-exposed membranes were used for quantification. Results are expressed as ratio ataxin-3/actin ($n = 6$ for each experimental set). Values are expressed as mean ± standard error of the mean. *$P < 0.05$ (paired Student's *t*-test). (**D**) Each ubiquitin lane was normalized according to the amount loaded (actin). Quantification was performed at the aggregates level (stacking gel, top to #). Results are expressed as ratio ubiquitin/actin. Values are expressed as mean ± standard error of the mean. **$P < 0.01$ (paired Student's *t*-test). (**E–H**) Lentiviral-based Machado–Joseph disease rat model. (**E**) Schematic representation of stereotaxic injection of lentiviral vectors in the rat striata. Human mutant ataxin-3 with 72 glutamines was co-injected with human Beclin-1 or phosphate buffered saline in the contralateral hemisphere as control. (**F**) Immunohistochemical analysis of rat striatal sections upon mutant ataxin-3 expression with or without Beclin-1. The analyses were performed at 4 weeks ($n = 8$, left) and 8 weeks ($n = 8$, right) post-injection, by staining for ataxin-3-positive inclusions (upper, scale bar = 200 μm and 20 μm, respectively) and ubiquitin-positive inclusions (lower, scale bar = 20 μm). (**G** and **H**) Quantification of whole striata transduced with mutant ataxin-3. (**G**) Quantification of absolute number of mutant ataxin-3-positive inclusions at 4 weeks ($n = 8$, left) and 8 weeks ($n = 8$, right) post-injection. Values are expressed as mean ± standard error of the mean. *$P < 0.05$; **$P < 0.01$ (paired Student's *t*-test). (**H**) Quantification of ubiquitin-positive inclusions at 4 weeks ($n = 8$, left) and 8 weeks ($n = 8$, right) post-injection. Values are expressed as mean ± standard error of the mean. *$P < 0.05$; ***$P < 0.001$ (paired Student's *t*-test). Atx3 MUT = mutant ataxin-3; Atx3 WT = wild-type ataxin-3.

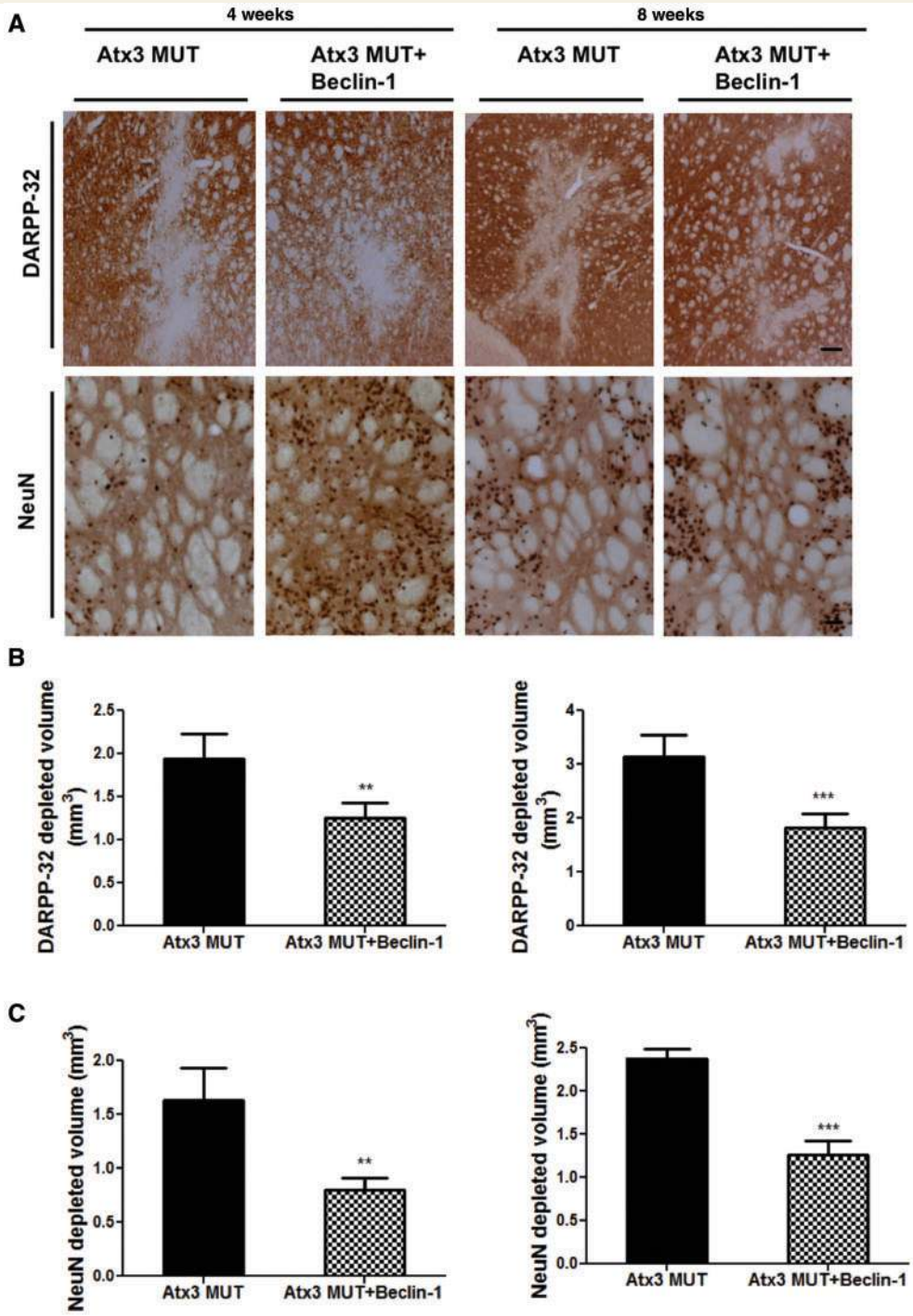

Figure 5 Beclin-1 overexpression reduces neurodysfunction in a rat model of Machado–Joseph disease. (**A**) Immunohistochemical analysis of rat striatal sections on human mutant ataxin-3 expression with or without Beclin-1 co-expression. The analyses were performed at 4 weeks ($n = 8$, *left*) and 8 weeks ($n = 8$, *right*) post-injection, by staining for the neuronal markers, dopamine- and cyclic AMP-regulated phosphoprotein of 32 000 kDa (DARPP-32, *upper*, scale bar = 200 μm) and neuronal nuclei (*lower*, scale bar = 50 μm). (**B** and **C**) Quantification of whole striata transduced with mutant ataxin-3. (**B**) Quantification of DARPP-32 depleted volume (mm^3) at 4 weeks ($n = 8$, *left*) and 8 weeks ($n = 8$, *right*) post-injection. Values are expressed as mean ± standard error of the mean. $^{**}P < 0.01$; $^{***}P < 0.001$ (paired Student's *t*-test). (**C**) Quantification of neuronal nuclei protein depleted volume (mm^3) at 4 weeks (*left*) and 8 weeks post-injection (*right*). Values are expressed as mean ± standard error of the mean. $^{**}P < 0.01$; $^{***}P < 0.001$ (paired Student's *t*-test). Atx3 MUT = mutant ataxin-3; NeuN = neuronal nuclei protein.

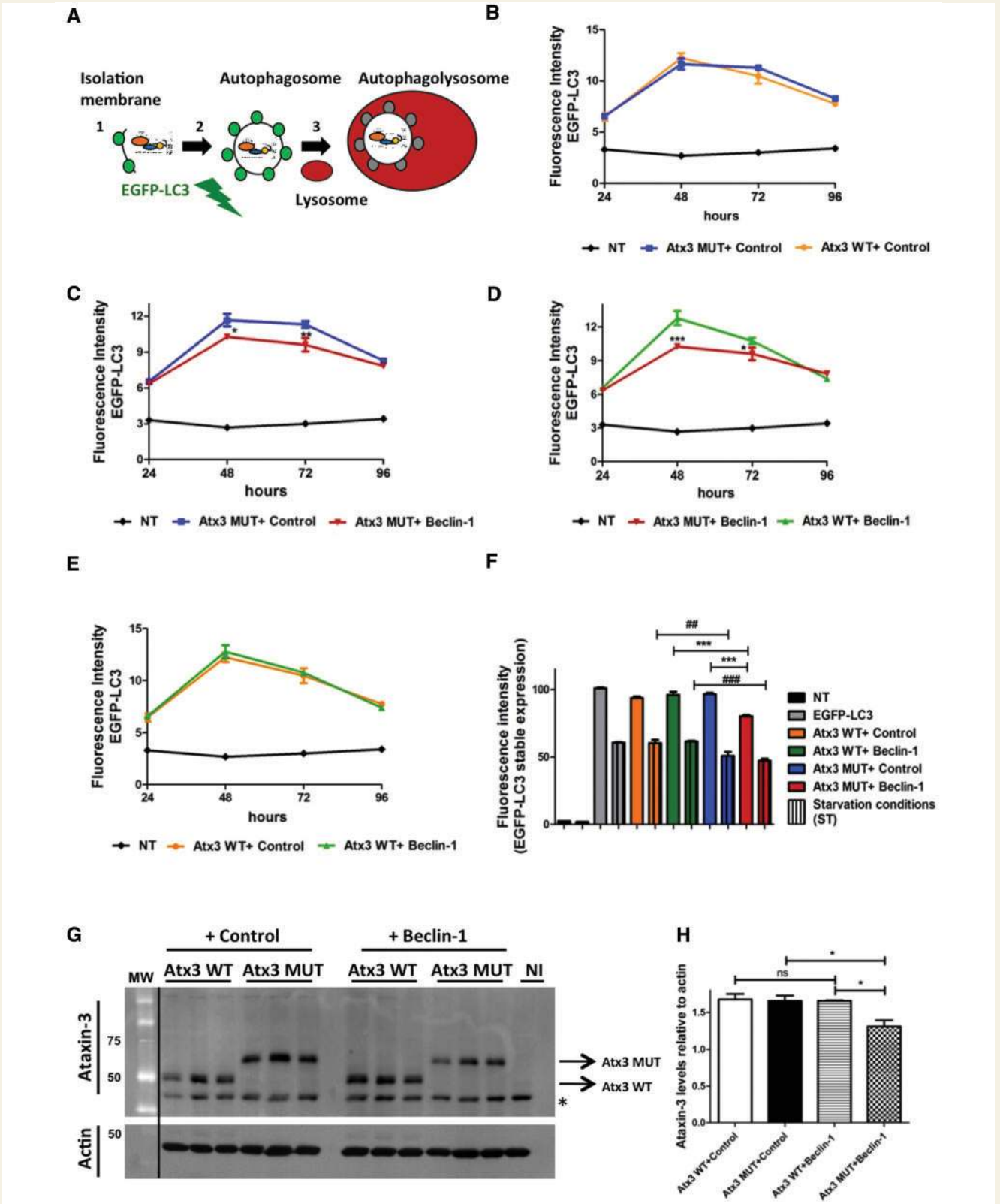

Figure 6 Beclin-1 selectively improves autophagosomal flux in mutant ataxin-3-expressing cells. (**A–F**) Flow cytometry analysis on live neuroblastoma cells (Neuro-2a) expressing enhanced green fluorescent protein-light chain 3. (**A**) Schematic representation of autophagosomal flux. The enhanced green fluorescent protein-light chain 3 protein (green dots) is incorporated in the autophagosomal membrane (Step 1 to 2) and fluorescence is emitted. Once inside lysosomes (Step 3) the enhanced green fluorescent protein-light chain 3 protein no longer emits fluorescence. A decrease in the enhanced green fluorescent protein-light chain 3 fluorescence intensity translates an increase in the autophagosomal flux and consequently in protein degradation. (**B–E**) Transient enhanced green fluorescent protein-light chain 3

(continued)

autophagosomal degradation continued to be more relevant for the mutant ataxin-3 ($n = 3$, Fig. 6F, blue-starvation conditions; 50.96 ± 2.84 versus 60.39 ± 2.39 in wild-type ataxin-3, orange-starvation conditions, both control treated; $P < 0.01$). With concomitant beclin-1 expression, the degradation was even more prominent for the mutant compared to the wild-type ataxin-3 ($n = 3$, Fig. 6F, red-starvation conditions; 47.33 ± 1.45 versus 61.58 ± 0.61 for wild-type ataxin-3, green-starvation conditions; $P < 0.001$). Next, to further infer about autophagic preferential clearance of mutant versus wild-type ataxin-3, a western blot analysis of Neuro-2a cells co-infected with ataxin-3 plus beclin-1/control vectors was performed 2 weeks post-infection (Fig. 6G and H). In the presence of beclin-1, mutant ataxin-3 was more extensively cleared than wild-type ataxin-3 ($n = 3$, Fig. 6G and H; 1.31 ± 0.08 versus 1.66 ± 0.009 for wild-type ataxin-3; $P < 0.05$). In conformity, a decrease in mutant ataxin-3 levels upon beclin-1-treatment was also observed when compared to control-treated ($n = 3$, Fig. 6G and H; 1.31 ± 0.08 versus 1.66 ± 0.07 in controls; $P < 0.05$).

Altogether, these data show that beclin-1 is able to stimulate autophagosomal flux and therefore promote protein clearance, with selective higher degradation efficiency for mutant, as compared to wild-type, ataxin-3.

Discussion

In this study, we provide evidence of an impairment of the autophagy pathway in advanced Machado–Joseph disease and demonstrate that an early stimulation of the beclin-1 autophagic pathway increases mutant ataxin-3 clearance and reduce its neurotoxicity.

In the first part of the study, we have shown that the disease modifies endogenous levels of autophagic proteins, in tissue of patients with Machado–Joseph disease, rats (Alves *et al*., 2008*b*) and transgenic mice (Goti *et al*., 2004). The accumulation of autophagosomes in brains of patients with Machado–Joseph disease, as well as in advanced stages of the rat and mouse model, suggests that autophagy is compromised in more advanced stages of the disease, in accordance with what has been described for Alzheimer's (Nixon *et al*., 2005; Yu *et al*., 2005; Jaeger *et al*., 2010) and Parkinson's diseases (Crews *et al*., 2010). In healthy neurons, the autophagy pathway is constitutively active and highly efficient and therefore the autophagic accumulation here observed most likely arises from insufficient clearance of autophagosomes (Boland *et al*., 2008). Additional analyses in the Machado–Joseph disease rodent models suggested that the autophagic cargo recognition step is functional, as ubiquitinated ataxin-3 inclusions were detected by the autophagosomal receptor p62 and found co-localized with light chain 3. This finding is of major importance, since p62 participates in the effective targeting of ubiquitinated proteins to autophagosomes (Bjorkoy *et al*., 2005; Kirkin *et al*., 2009). Despite the fact that the autophagy pathway is functional in early stages of disease, mutant proteins progressively accumulate along with the autophagosomes in a late stage, which means that the autophagy machinery probably reaches saturation when the amount of mutant protein synthesized is higher than the degradative capacity of the autophagy system (reviewed in Cuervo, 2004; Wong and Cuervo, 2010). In agreement with that hypothesis, levels of the autophagic protein beclin-1 were found to be decreased in fibroblasts from patients with Machado–Joseph disease and rodent models for the disease. This finding is in agreement with what previously described for Huntington's (Shibata *et al*., 2006) and Alzheimer's diseases (Pickford *et al*., 2008; Jaeger *et al*., 2010). A decrease in beclin-1 levels has been also described in ageing (Shibata *et al*., 2006) and there is evidence that the ageing-related decline of the autophagic function may be involved in the delayed onset of neurodegenerative diseases (Simonsen *et al*., 2008).

Figure 6 Continued
fluorescence intensity was measured at 24, 48, 72 and 96 h post-transfection ($n = 3$ for each experimental set and time-point) and is highlighted with a colour code depending on the experimental set. Basal fluorescence of Neuro-2a cells is also represented (NT, black). (**B**) Quantification of enhanced green fluorescent protein fluorescence intensity of cells expressing control-treated wild-type (orange) or mutant ataxin-3 proteins. No significant differences were observed between control-treated wild-type and mutant ataxin-3. Values are expressed as mean ± standard error of the mean. (**C**) Quantification of enhanced green fluorescent protein fluorescence intensity of cells expressing mutant ataxin-3 plus control (blue) or Beclin-1 (red). Values are expressed as mean ± standard error of the mean. $*P < 0.05$, for 48 h; $**P < 0.01$ for 72 h (two-way ANOVA, Bonferroni post-test). (**D**) Quantification of enhanced green fluorescent protein fluorescence intensity of cells expressing beclin-1-treated wild-type (green) and mutant ataxin-3 (red). Values are expressed as mean ± standard error of the mean. $*P < 0.05$, for 72 h; $***P < 0.001$, for 48 h (two-way ANOVA, Bonferroni post-test). (**E**) Quantification of enhanced green fluorescent protein fluorescence intensity of cells expressing wild-type ataxin-3 plus Beclin-1 (green) or control (orange). No significant differences were observed. (**F**) Flow cytometry analysis of Neuro-2a stably expressing enhanced green fluorescent protein-light chain 3. Cells expressing enhanced green fluorescent protein-light chain 3 were transfected with ataxin-3 and beclin-1/control constructs. The fluorescence intensity was measured at 48 h post-transfection ($n = 3$ for each experimental set). Starvation conditions (ST, vertical stripes), used as a positive control for autophagy, were performed by starving cells 3 h prior the analysis. Values are expressed as mean ± standard error of the mean. $***P < 0.001$ relative to complete medium conditions; $^{\#\#}P < 0.01$ and $^{\#\#\#}P < 0.001$ relative to starvation conditions (one-way ANOVA, Bonferroni post-test). (**G** and **H**) Western blot analysis of Neuro-2a cells double-infected with ataxin-3 and beclin-1/control constructs. Analysis was performed 2 weeks post-infection. (**G**) Representative membranes probed with the ataxin-3 and actin antibodies; *endogenous murine ataxin-3. (**H**) Optical densitometry analysis. Results are expressed as ratio ataxin-3/actin. Values are expressed as mean ± standard error of the mean; $*P < 0.05$ (one-way ANOVA, Bonferroni post-test). Altogether these data show that beclin-1 stimulates autophagosomal flux and concomitant selective mutant ataxin-3 clearance. Atx3 MUT = mutant ataxin-3; EGFP-LC3 = enhanced green fluorescent protein = light chain 3; Atx3 WT = wild-type ataxin-3.

Beclin-1 and mammalian target of rapamycin are part of large protein complexes, which regulate the two signalling pathways controlling autophagy (Yorimitsu and Klionsky, 2005). Inhibition of the mammalian target of rapamycin complex activates autophagy while the beclin-1 complex directly activates autophagosome formation (Yorimitsu and Klionsky, 2005). In our study, beclin-1 overexpression proved to achieve a robust effect regarding the stimulation of the autophagosomal flux, mutant ataxin-3 clearance and neuroprotection. Beclin-1 mediated clearance of soluble and insoluble toxic forms of mutant ataxin-3, leading ultimately to neuroprotective effects. Furthermore, the fact that beclin-1-mediated clearance was more pronounced for the mutant relative to the wild-type ataxin-3 proves that this pathway can be selective for the degradation of mutant proteins, challenging the original idea of autophagy as a bulk degradation system (reviewed in Rubinsztein, 2006).

While completing the experiments for this article, beneficial effects of autophagy stimulation in a model of Machado–Joseph disease, through administration of a rapamycin analogue, temsirolimus, were reported (Menzies *et al*., 2009). Our study not only supports those results but also reinforces them with a more mechanistic analysis and an autophagy-specific approach. Since mammalian target of rapamycin is a protein kinase that regulates multiple important cellular functions (Wullschleger *et al*., 2006), potential non-specific effects may be obtained with an mammalian target of rapamycin inhibition strategy. Furthermore, rapamycin itself has been described to decrease polyQ protein synthesis (King *et al*., 2008; Li *et al*., 2008). On the other hand, beclin-1 interacts with the class III phosphatidylinositol 3-kinase/VPS-34 complex and activates autophagy through a different mechanism, which directly activates autophagic-related proteins and therefore should allow autophagy stimulation in a specific manner (Cao and Klionsky, 2007).

In conclusion, this study correlates the reduced levels of beclin-1 protein with a late impairment of the autophagy pathway in Machado–Joseph disease and shows that selective activation of the beclin-1-autophagic pathway promotes degradation of mutant ataxin-3, identifying this pathway as a molecular target of major importance for therapy in Machado–Joseph disease.

Acknowledgements

We thank Dr Tamotsu Yoshimory for providing the enhanced green fluorescent protein-light chain 3 construct, Dr Beth Levine for the Beclin-1 construct, Dr Olinda Garcia for post-mortem human brain tissue; and the technical assistance of Dr Luísa Cortes (confocal microscopy), Sylvain Martineau (real-time PCR), Aurélie Delzor (*in vivo* experiments), Carole Malgorn (primary cell cultures), Clévio Nóbrega (Neuro-2 A cell culture) and Sara Trabulo/ Dr Isabel Nunes (flow cytometry).

Funding

This work was supported by the Portuguese Foundation for Science and Technology (PTDC/SAU-FCF/70384/2006 and PTDC/SAU-NEU/099307/2008), the National Ataxia Foundation (NAF Research Award 2010), the *Commissariat à L'Energie Atomique* (CEA) and the Association Française pour les Myopathies (AFM; SB/NF/2010/2008 Number 15079CA). Isabel Nascimento-Ferreira, Lígia Sousa-Ferreira, Sandro Alves and Isabel Onofre were supported by the Portuguese Foundation for Science and Technology.

Supplementary material

Supplementary material is available at *Brain* online.

References

Alves S, Nascimento-Ferreira I, Auregan G, Hassig R, Dufour N, Brouillet E, et al. Allele-specific RNA silencing of mutant ataxin-3 mediates neuroprotection in a rat model of Machado-Joseph disease. PLoS One 2008a; 3: e3341.

Alves S, Regulier E, Nascimento-Ferreira I, Hassig R, Dufour N, Koeppen A, et al. Striatal and nigral pathology in a lentiviral rat model of Machado-Joseph disease. Hum Mol Genet 2008b; 17: 2071–83.

Bampton ET, Goemans CG, Niranjan D, Mizushima N, Tolkovsky AM. The dynamics of autophagy visualized in live cells: from autophagosome formation to fusion with endo/lysosomes. Autophagy 2005; 1: 23–36.

Bjorkoy G, Lamark T, Brech A, Outzen H, Perander M, Overvatn A, et al. p62/SQSTM1 forms protein aggregates degraded by autophagy and has a protective effect on huntingtin-induced cell death. J Cell Biol 2005; 171: 603–14.

Boland B, Kumar A, Lee S, Platt FM, Wegiel J, Yu WH, et al. Autophagy induction and autophagosome clearance in neurons: relationship to autophagic pathology in Alzheimer's disease. J Neurosci 2008; 28: 6926–37.

Cao Y, Klionsky DJ. Physiological functions of Atg6/Beclin 1: a unique autophagy-related protein. Cell Res 2007; 17: 839–49.

Chai Y, Berke SS, Cohen RE, Paulson HL. Poly-ubiquitin binding by the polyglutamine disease protein ataxin-3 links its normal function to protein surveillance pathways. J Biol Chem 2004; 279: 3605–11.

Crews L, Spencer B, Desplats P, Patrick C, Paulino A, Rockenstein E, et al. Selective molecular alterations in the autophagy pathway in patients with Lewy body disease and in models of alpha-synucleinopathy. PLoS One 2010; 5: e9313.

Cuervo AM. Autophagy: in sickness and in health. Trends Cell Biol 2004; 14: 70–7.

de Almeida LP, Ross CA, Zala D, Aebischer P, Deglon N. Lentiviral-mediated delivery of mutant huntingtin in the striatum of rats induces a selective neuropathology modulated by polyglutamine repeat size, huntingtin expression levels, and protein length. J Neurosci 2002; 22: 3473–83.

Deglon N, Tseng JL, Bensadoun JC, Zurn AD, Arsenijevic Y, Pereira de Almeida L, et al. Self-inactivating lentiviral vectors with enhanced transgene expression as potential gene transfer system in Parkinson's disease. Hum Gene Ther 2000; 11: 179–90.

Doss-Pepe EW, Stenroos ES, Johnson WG, Madura K. Ataxin-3 interactions with rad23 and valosin-containing protein and its associations with ubiquitin chains and the proteasome are consistent with a role in ubiquitin-mediated proteolysis. Mol Cell Biol 2003; 23: 6469–83.

Duenas AM, Goold R, Giunti P. Molecular pathogenesis of spinocerebellar ataxias. Brain 2006; 129: 1357–70.

Goti D, Katzen SM, Mez J, Kurtis N, Kiluk J, Ben-Haiem L, et al. A mutant ataxin-3 putative-cleavage fragment in brains of patients

with Machado–Joseph disease and transgenic mice is cytotoxic above a critical concentration. J Neurosci 2004; 24: 10266–79.
Hara T, Nakamura K, Matsui M, Yamamoto A, Nakahara Y, Suzuki-Migishima R, et al. Suppression of basal autophagy in neural cells causes neurodegenerative disease in mice. Nature 2006; 441: 885–9.
Ichimura Y, Komatsu M. Selective degradation of p62 by autophagy. Semin Immunopathol 2010; 32: 431–6.
Jaeger PA, Pickford F, Sun CH, Lucin KM, Masliah E, Wyss-Coray T. Regulation of amyloid precursor protein processing by the Beclin 1 complex. PLoS One 2010; 5: e11102.
Jia K, Hart AC, Levine B. Autophagy genes protect against disease caused by polyglutamine expansion proteins in Caenorhabditis elegans. Autophagy 2007; 3: 21–5.
Kabeya Y, Mizushima N, Ueno T, Yamamoto A, Kirisako T, Noda T, et al. Light chain 3, a mammalian homologue of yeast Apg8p, is localized in autophagosome membranes after processing. EMBO J 2000; 19: 5720–8.
Kawaguchi Y, Okamoto T, Taniwaki M, Aizawa M, Inoue M, Katayama S, et al. CAG expansions in a novel gene for Machado–Joseph disease at chromosome 14q32.1. Nat Genet 1994; 8: 221–8.
Kegel KB, Kim M, Sapp E, McIntyre C, Castano JG, Aronin N, et al. Huntingtin expression stimulates endosomal-lysosomal activity, endosome tubulation, and autophagy. J Neurosci 2000; 20: 7268–78.
King MA, Hands S, Hafiz F, Mizushima N, Tolkovsky AM, Wyttenbach A. Rapamycin inhibits polyglutamine aggregation independently of autophagy by reducing protein synthesis. Mol Pharmacol 2008; 73: 1052–63.
Kirkin V, McEwan DG, Novak I, Dikic I. A role for ubiquitin in selective autophagy. Mol Cell 2009; 34: 259–69.
Komatsu M, Waguri S, Chiba T, Murata S, Iwata J, Tanida I, et al. Loss of autophagy in the central nervous system causes neurodegeneration in mice. Nature 2006; 441: 880–4.
Komatsu M, Waguri S, Koike M, Sou YS, Ueno T, Hara T, et al. Homeostatic levels of p62 control cytoplasmic inclusion body formation in autophagy-deficient mice. Cell 2007; 131: 1149–63.
Li X, Li H, Li XJ. Intracellular degradation of misfolded proteins in polyglutamine neurodegenerative diseases. Brain Res Rev 2008; 59: 245–52.
Liang XH, Jackson S, Seaman M, Brown K, Kempkes B, Hibshoosh H, et al. Induction of autophagy and inhibition of tumorigenesis by beclin 1. Nature 1999; 402: 672–6.
Menzies FM, Huebener J, Renna M, Bonin M, Riess O, Rubinsztein DC. Autophagy induction reduces mutant ataxin-3 levels and toxicity in a mouse model of spinocerebellar ataxia type 3. Brain 2009; 133: 93–104.
Mizushima N, Yoshimori T, Levine B. Methods in mammalian autophagy research. Cell 2010; 140: 313–26.
Nixon RA, Wegiel J, Kumar A, Yu WH, Peterhoff C, Cataldo A, et al. Extensive involvement of autophagy in Alzheimer disease: an immuno-electron microscopy study. J Neuropathol Exp Neurol 2005; 64: 113–22.
Pankiv S, Clausen TH, Lamark T, Brech A, Bruun JA, Outzen H, et al. p62/SQSTM1 binds directly to Atg8/light chain 3 to facilitate degradation of ubiquitinated protein aggregates by autophagy. J Biol Chem 2007; 282: 24131–45.
Pickford F, Masliah E, Britschgi M, Lucin K, Narasimhan R, Jaeger PA, et al. The autophagy-related protein beclin 1 shows reduced expression in early Alzheimer disease and regulates amyloid beta accumulation in mice. J Clin Invest 2008; 118: 2190–9.
Rubinsztein DC. The roles of intracellular protein-degradation pathways in neurodegeneration. Nature 2006; 443: 780–6.
Schmidt T, Landwehrmeyer GB, Schmitt I, Trottier Y, Auburger G, Laccone F, et al. An isoform of ataxin-3 accumulates in the nucleus of neuronal cells in affected brain regions of Spinocerebelar ataxia type 3 patients. Brain Pathol 1998; 8: 669–79.
Shibata M, Lu T, Furuya T, Degterev A, Mizushima N, Yoshimori T, et al. Regulation of intracellular accumulation of mutant Huntingtin by Beclin 1. J Biol Chem 2006; 281: 14474–85.
Shvets E, Fass E, Elazar Z. Utilizing flow cytometry to monitor autophagy in living mammalian cells. Autophagy 2008; 4: 621–8.
Simonsen A, Cumming RC, Brech A, Isakson P, Schubert DR, Finley KD. Enhanced neuronal autophagy promotes longevity and oxidant resistance in drosophila. Autophagy 2008; 4: 176–84.
Spencer B, Potkar R, Trejo M, Rockenstein E, Patrick C, Gindi R, et al. Beclin 1 gene transfer activates autophagy and ameliorates the neurodegenerative pathology in alpha-synuclein models of Parkinson's and Lewy body diseases. J Neurosci 2009; 29: 13578–88.
Takacs-Vellai K, Vellai T, Puoti A, Passannante M, Wicky C, Streit A, et al. Inactivation of the autophagy gene bec-1 triggers apoptotic cell death in C. elegans. Curr Biol 2005; 15: 1513–7.
Vellai T. Autophagy genes and ageing. Cell Death Differ 2009; 16: 94–102.
Williams A, Jahreiss L, Sarkar S, Saiki S, Menzies FM, Ravikumar B, et al. Aggregate-prone proteins are cleared from the cytosol by autophagy: therapeutic implications. Curr Top Dev Biol 2006; 76: 89–101.
Wong E, Cuervo AM. Autophagy gone awry in neurodegenerative diseases. Nat Neurosci 2010; 13: 805–11.
Wullschleger S, Loewith R, Hall MN. TOR signaling in growth and metabolism. Cell 2006; 124: 471–84.
Yorimitsu T, Klionsky DJ. Autophagy: molecular machinery for self-eating. Cell Death Differ 2005; 12 (Suppl 2): 1542–52.
Yu WH, Cuervo AM, Kumar A, Peterhoff CM, Schmidt SD, Lee JH, et al. Macroautophagy–a novel Beta-amyloid peptide-generating pathway activated in Alzheimer's disease. J Cell Biol 2005; 171: 87–98.
Zala D, Benchoua A, Brouillet E, Perrin V, Gaillard MC, Zurn AD, et al. Progressive and selective striatal degeneration in primary neuronal cultures using lentiviral vector coding for a mutant huntingtin fragment. Neurobiol Dis 2005; 20: 785–98.
Zeng X, Overmeyer JH, Maltese WA. Functional specificity of the mammalian Beclin-Vps34 PI 3-kinase complex in macroautophagy versus endocytosis and lysosomal enzyme trafficking. J Cell Sci 2006; 119: 259–70.
Zoghbi HY. Spinocerebellar ataxias. Neurobiol Dis 2000; 7: 523–7.